Journal of Geophysical Research: Oceans

RESEARCH ARTICLE
10.1029/2017JC013405

Key Points:
- Shelf-scale submarine groundwater discharge was estimated using Ra
- Submarine groundwater discharge is an important source of nutrients and carbon on shelves
- Submarine groundwater discharge must be considered in shelf biogeochemical studies considering their wide occurrences

Supporting Information:
- Supporting Information S1
- Data Set S1
- Data Set S2
- Data Set S3

Correspondence to:
G. Wang,
gzhwang@xmu.edu.cn

Citation:
Tan, E., Wang, G., Moore, W. S., Li, Q., & Dai, M. (2018). Shelf-scale submarine groundwater discharge in the northern South China Sea and East China Sea and its geochemical impacts. *Journal of Geophysical Research: Oceans*, *123*, 2997–3013. https://doi.org/10.1029/2017JC013405

Received 5 SEP 2017
Accepted 2 APR 2018
Accepted article online 6 APR 2018
Published online 26 APR 2018

Shelf-Scale Submarine Groundwater Discharge in the Northern South China Sea and East China Sea and Its Geochemical Impacts

Ehui Tan[1,2], Guizhi Wang[1,2,3], Willard S. Moore[4], Qing Li[1,2], and Minhan Dai[1,2]

[1]State Key Laboratory of Marine Environmental Science, Xiamen University, Xiamen, China, [2]College of Ocean and Earth Sciences, Xiamen University, Xiamen, China, [3]Fujian Provincial Key Laboratory for Coastal Ecology and Environmental Studies, Xiamen University, Xiamen, China, [4]Department of Earth and Ocean Sciences, University of South Carolina, Columbia, SC, USA

Abstract To evaluate biogeochemical impacts of shelf-scale submarine groundwater discharge (SGD), the northern South China Sea (NSCS) and the East China Sea (ECS) shelf were chosen for this study. Based on a three end-member mixing model and a Ra box model, SGD fluxes on NSCS (west and east of the Pearl River Estuary, WPRE and EPRE, respectively) and ECS shelf in winter were estimated to be 3.8–9.5 $\times$ 10^9, 1.4–2.2 $\times$ 10^9 and 0.7–2.2 $\times 10^{10}$ m^3 d^{-1}, respectively. Our results were equivalent to the SGD flux to the entire Mediterranean Sea, and were an order of magnitude greater than fluxes to the South Atlantic Bight. SGD associated nutrient fluxes into WPRE, EPRE and ECS were almost in the same order of magnitude, 0.2–2.4 $\times$ 10^3 mol m^{-1} d^{-1} for dissolved inorganic nitrogen, 1.2–9.8 mol m^{-1} d^{-1} for soluble reactive phosphorus, and 0.4–3.4 $\times$ 10^3 mol m^{-1} d^{-1} for dissolved silicate. Moreover, SGD delivered 1.1–2.8 $\times$ 10^4, 0.6–0.9 $\times$ 10^4, 1.7–5.1 $\times$ 10^4 mol m^{-1} d^{-1} dissolved inorganic carbon and 1.1–2.7 $\times$ 10^4, 0.5–0.8 $\times$ 10^4, 1.6–4.8 $\times$ 10^4 mol m^{-1} d^{-1} total alkalinity to WPRE, EPRE and ECS, respectively. Shelf-scale SGD is a significant source of nutrients and carbon, and may pose great impacts on regional marine ecosystems.

1. Introduction

Submarine groundwater discharge (SGD), which has been defined as any and all flow of water on continental margins from the seabed to the coastal ocean, regardless of fluid composition and driving forces, contains fresh water derived from land and saline water from seawater exchange (Burnett et al., 2003). In the last few decades, there has been growing attention to SGD and associated dissolved solute fluxes into coastal oceans (Charette & Buesseler, 2004; Kohout & Kolipinski, 1967; Liu et al., 2012, 2014; Moore, 1998; Street et al., 2008; Valiela et al., 1990; Wang et al., 2015).

SGD is a significant component of land-ocean interactions and material transport pathways for coastal systems (Moore, 2010a). Abundant dissolved solutes are carried by SGD, for example dissolved inorganic nitrogen (DIN), soluble reactive phosphorus (SRP), dissolved silicate (DSi), dissolved inorganic carbon (DIC), total alkalinity (TA), and trace metals, with concentrations that are often an order of magnitude higher than those in seawater (Charette & Buesseler, 2004; Sanders et al., 2012). Thus, SGD may have great impacts on local ecosystems and biogeochemical cycles in coastal zones. Recent studies have found that nutrients from SGD can drive harmful algal blooms, coastal eutrophication, and coastal acidification. Smith and Swarzenski (2012) discussed the relationship between submarine groundwater-borne nutrient fluxes and recurrent harmful algal blooms on the west-central Florida coast. They found that SGD-derived loads could narrow the deficit between observed nutrients and bloom demands even if it was not the dominant nutrients source. According to Lee et al. (2009), the large and continuous supply of inorganic nutrients through SGD may play an important role in eutrophication and the occurrence of red tides in Masan Bay in Korea. Wang et al. (2014) demonstrated that SGD could be a contributor to acidification of a coastal fringing reef system in Sanya Bay in the South China Sea.

In general, SGD studies are mainly focused on coastal zones, including estuaries, bays, and islands, such as Jiulong River estuary (Wang et al., 2015), West Neck Bay (Dulaiova et al., 2006), Yeongil Bay (Kim et al., 2007), and Balearic Islands (Garcia-Solsona et al., 2009). Few studies have quantified SGD flux in shelf-scale regions

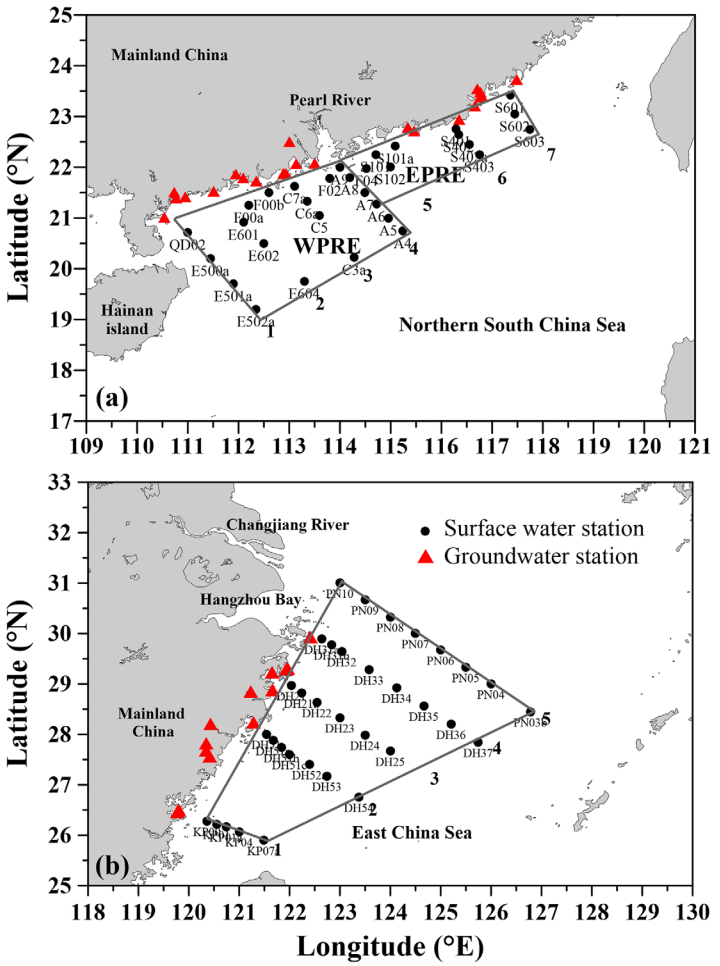

Figure 1. Sampling sites on (a) the northern South China Sea shelf and (b) the East China Sea shelf. The cross-shelf transects are marked by numbers 1–7 in NSCS and 1–5 in ECS. Gray quadrangles show the study areas; WPRE and EPRE are separated by transect 4 in NSCS.

and evaluated the geochemical impacts of SGD-associated material fluxes on shelf waters, especially the influence on the carbon budget and biological production (Gu et al., 2012; Liu et al., 2012, 2014). We thus chose the northern South China Sea (NSCS) shelf and East China Sea (ECS) shelf, two major river-dominated shelves off the China mainland, to quantify the SGD flux using radium isotopes and provide a quantitative and comparative assessment on how SGD-derived materials affect the shelf water.

Four naturally occurring radium isotopes, two short-lived isotopes (^{223}Ra and ^{224}Ra) and two long-lived isotopes (^{226}Ra and ^{228}Ra), are found to be powerful tools to trace SGD and water masses (Moore, 1999). Ra isotopes are generated from decay of their thorium parents. Ra is largely particle-bound in fresh water, but desorbs from particles in contact with saline water (Moore, 2010a). Thus, Ra is highly enriched in salty coastal groundwater relative to seawater, and small inputs of SGD can produce a strong Ra signal.

To estimate SGD fluxes in winter, we conducted two cruises in the study regions and collected groundwater samples along the NSCS and ECS coasts (Figure 1). Based on radium isotopes, ^{226}Ra and ^{228}Ra, and salinity in groundwater and seawater, a three end-member mixing model and a Ra box model were applied to quantify the SGD fluxes and associated nutrients and carbon fluxes on the shelf of NSCS and ECS. From these studies the geochemical impacts of SGD were evaluated.

2. Materials and Methods

2.1. Study Area

The Pearl River and Yangtze River are the dominant rivers in the NSCS shelf and ECS shelf, respectively; the effects of other small rivers on the discharge of water and sediments into the study areas are insignificant (Ministry of Water Resources of PRC, 2010; Hong et al., 2016; Mao & Shen, 2001; Wang et al., 2010) (supporting information Table S1). The NSCS shelf is a typical river dominated region, which is influenced by fresh water from the largest river in southern China, the Pearl River. It has an annual freshwater discharge of 3.26×10^{11} m^3 yr^{-1} (Guo et al., 2008). After leaving the Pearl River Estuary, the river plume moves westward into the NSCS shelf and reaches as far south as the Hainan Island, driven by the northeasterly monsoon in the winter dry season (Dong et al., 2004). The surface sediments on the NSCS continental shelf show grain size gradations from gravel inshore to silt offshore (Luo et al., 1985). The region along the shoreline of the NSCS is composed of thick and widespread quaternary deposits, with terrigenous and biogenous detritus as the major components (Zhang et al., 2003).

The Yangtze River is the third longest river in the world and the largest river in China with an annual mean freshwater discharge of 0.9×10^{12} m^3 yr^{-1} (Milliman & Meade, 1983). The freshwater discharge has a significant seasonal variation, with a maximum in July to August and a minimum in January to February each year. In winter the river plume is confined to move southwestward along the east coast of China under the strong northeasterly monsoon winds, where it converges with the Yellow sea coastal current to form the Min-Zhe coastal current (MZCC) along the inner shelf (Liu et al., 2006). On the outer shelf, the Taiwan Warm Current (TWWC), flows northward with warm and high salinity water, which originates mainly from the Kuroshio Current (Beardsley et al., 1985; Lee & Chao, 2003; Lian et al., 2016; Liu et al., 2006); This current dominates the outer continental shelf during all seasons.

2.2. Sampling and Pretreatment

Our cruises were carried out in the winter dry season from 6 to 25 January 2010 in the NSCS, and from 29 December 2009 to 4 January 2010 in the ECS on-board R/V Dongfanghong II. The NSCS shelf was divided

into two parts, the west and east of the Pearl River Estuary, WPRE and EPRE, respectively, based on different water masses (Figure 1a). The other cruise was conducted in the ECS from the Yangtze River mouth and southward to the east of Taiwan Island, including five shore perpendicular transects, where water depths and distance offshore ranged from 23 to 200 m and 40 to 460 km, respectively (Figure 1b).

Large volume samples (offshore 200 L) for Ra isotopes were pumped from the sea surface into a polypropylene container. Then the water temperature and salinity were directly measured using a WTW analyzer, before the water was pumped with a small submersible pump through a 1 μm cartridge filter, then passed through a column of MnO_2 coated acrylic fiber (Mn fiber) at a flow rate less than 1 L per minute to remove Ra (Moore, 1976; Moore et al., 1985). Surface water samples for nutrients, DIC and TA were taken from Niskin bottles mounted on a rosette equipped with a calibrated Sea-Bird Electronics (SBE)-19-plus conductivity-temperature-depth (CTD) recorder. Profiles of temperature and salinity at each station were recorded by CTD.

Coastal groundwater was sampled from wells and sandy beaches along the NSCS and ECS coasts using peristaltic pump and PushPoint sampler (Moore et al., 2006) (Figure 1). The sample volume for Ra was 8 L, and the sample was processed using the same preconcentration method as for seawater. Total alkalinity (TA), dissolved inorganic carbon (DIC) and major dissolved nutrients (DIN, DSi, SRP) samples were collected and measured in the laboratory. Both TA and DIC samples were poisoned upon collection using 50 μL saturated $HgCl_2$ solution, and stored in 100 mL polyethylene bottles and 40 mL borosilicate glass vials, respectively. Samples for dissolved nutrients were filtered through 0.45 μm filters and stored in 100 mL polyethylene bottles. DIN and SRP samples were stored at −20°C, and DSi samples were stored at 4°C after being preserved with chloroform upon collection.

2.3. Measurements of Ra Isotopes

There are four naturally-occurring radium isotopes: two short-lived, ^{223}Ra (half-life = 11.4 day) and ^{224}Ra (half-life = 3.66 day), and two long-lived, ^{226}Ra (half-life = 1,600 years) and ^{228}Ra (half-life = 5.75 year), which are useful in tracing oceanographic processes (Moore, 2010a). ^{223}Ra and ^{224}Ra were measured using radium delayed coincidence counters (RaDeCC), a proven, precise and fast way to measure ^{223}Ra and ^{224}Ra in water samples (Moore, 2003; Moore & Arnold, 1996; Rapaglia et al., 2012). The principle for the RaDeCC system is that the system can utilize the difference in decay constants of the short-lived Po daughters of ^{219}Rn and ^{220}Rn to identify alpha particles derived from ^{219}Rn and ^{220}Rn decay and hence to determine activities of ^{223}Ra and ^{224}Ra on the Mn fiber (Moore, 2008; Moore & Cai, 2013).

In the laboratory, the Mn-fiber was washed with Ra-free deionized water to remove sea salts, partially dried to adjust to an appropriate moisture content and placed in a closed loop helium circulation system. Helium was circulated through the RaDeCC system to sweep the ^{219}Rn and ^{220}Rn generated by ^{223}Ra and ^{224}Ra that were absorbed on the Mn-fiber through a 1.1 L scintillation cell (Lucas, 1957), where alpha particles from the decay of Rn and daughters were recorded with a photomultiplier tube (PMT) attached to the scintillation cell. The signals from the PMT were routed to the RaDeCC system (Giffin et al., 1963; Moore & Arnold, 1996). The samples were remeasured after three weeks to determine the activity of ^{228}Th to correct for supported ^{224}Ra activity.

After ^{223}Ra, ^{224}Ra and ^{228}Th were measured, the Mn-fibers were leached with a mixture of 1 M hydrochloric acid solution and 1 M hydroxylamine hydrochloride solution at 80–90°C to remove Ra. Then ^{226}Ra and ^{228}Ra in the solution were co-precipitated with $BaSO_4$ and the precipitate was sealed in a small counting vial for 21 days to insure ^{222}Rn equilibration prior to being measured using a Canberra germanium well-type gamma detectors (Moore, 1984).

Standards prepared from ^{227}Ac and ^{232}Th were used to calibrate ^{223}Ra-^{219}Rn and ^{224}Ra-^{220}Rn measurements, respectively. The standards for ^{226}Ra and ^{228}Ra measurements were from International Atomic Energy Agency. The errors for Ra isotopes measurements were less than 10% based on propagation of counting statistics and counter calibration (Moore, 2008; Moore & Cai, 2013).

2.4. Measurements of TA, DIC, and Major Nutrients

TA was determined with Gran titration on a 25 mL water sample using a Kloehn digital syringe pump at a precision of 0.1%. DIC was measured with infrared detection at a precision of 0.1%-0.3% (Cai & Wang, 1998). The standard seawater from Andrew G. Dickson's lab was used to calibrate the system at the precision of 2 μmol kg^{-1} for both TA and DIC measurement (Cai et al., 2004; Zhai et al., 2007).

Nitrite (NO_2^-), nitrate (NO^-) and ammonium (NH_4^+) were measured using routine spectrophotometric methods with a Technicon AA3 Auto-Analyzer (Bran-Luebbe, GmbH) (Han et al., 2012). The detection limits were 0.02, 0.07 and 0.16 μM, respectively. DIN is the total sum of NO_2^-, NO_3^- and NH_4^+. SRP and DSi were measured using typical spectrophotometric methods with a precision of 2% and 2.8%, respectively (Dai et al., 2008; Han et al., 2012).

2.5. Methods

2.5.1. Box Model

A box model for long-lived Ra has been frequently used to quantify the SGD flux (Charette et al., 2008; Kwon et al., 2014; Smoak et al., 2012). Under the assumption of steady state, the sinks of Ra in the study region must be balanced by the Ra sources. In addition to SGD, other Ra sources on the shelf include local river inputs (dissolved and that desorbed from particles) and diffusion from shelf sediments (including the effects of bioturbation). Ra carried by alongshore transport can be a source or a sink depending on the difference of Ra fluxes between the boundary transects in the box. The sink comes from mixing with offshore water. Decay of long-lived Ra was ignored due to their relatively long half-lives compared to the time scale of mixing on the shelf. Therefore, the Ra mass balance model can be written as follows:

$$\frac{{}^{i}I}{\tau} = [\sum(Q_{riv} \times {}^{i}Ra_{riv})] + (A_{sed} \times {}^{i}F_{sed}) + (Q_{sgd} \times {}^{i}Ra_{sgd}) + [(Q_A \times {}^{i}Ra_A) - (Q_B \times {}^{i}Ra_B)] \quad (1)$$

where the left term is the total Ra exchange flux (dpm d^{-1}) with offshore seawater, ${}^{i}I$ represents the excess ^{226}Ra or ^{228}Ra inventory in the study regions and τ is the residence time (days). The right terms are the various Ra sources. $[\sum(Q_{riv} \times {}^{i}Ra_{riv})]$ denotes the Ra flux from local major rivers, Q_{riv} is the river discharge and ${}^{i}Ra_{riv}$ is the Ra end-member in each river estuary; $(A_{sed} \times {}^{i}F_{sed})$ is the diffusion flux from sediments, A_{sed} denotes the sediments areas where the mixed layer extends to the bottom and ${}^{i}F_{sed}$ is the Ra diffusion and bioturbation flux from sediments (dpm m^{-2} d^{-1}). $(Q_{sgd} \times {}^{i}Ra_{sgd})$ is the flux from SGD, Ra_{sgd} represents the average activities of Ra in the groundwater and Q_{sgd} is the SGD flux. Finally, $[(Q_A \times {}^{i}Ra_A) - (Q_B \times {}^{i}Ra_B)]$ represents the alongshore transport flux. The subscripts A and B denote the northern and southern boundaries of the box, Q is the net water flux through each boundary transect (m^3 d^{-1}) and Ra is the average Ra activity in each transect. We can calculate the flux of SGD (Q_{sgd}) after quantifying other terms.

The approach used in the southeastern U.S. continental shelf (Moore, 2007) was applied to evaluate the ^{226}Ra and ^{228}Ra inventories. Firstly, the excess ^{226}Ra and ^{228}Ra in the shelf water were obtained by subtracting the background oceanic Ra activities (7.44 and 3.09 dpm 100 L^{-1} for ^{226}Ra and ^{228}Ra at station A4 in the NSCS, 5.63 and 1.64 dpm 100 L^{-1} for ^{226}Ra and ^{228}Ra at station DH54 in the ECS, respectively). For the calculation of V_{SW}, the study area was divided into multiple triangle boxes connecting three adjacent study stations. The Ra inventory in each triangle box was calculated by multiplying the average excess Ra activities of the three adjacent stations by the volume of water in each triangle box. The calculation was based on the assumption that the surface samples were representative of the entire mixed layer. This assumption is supported by the mixed layer analysis shown in the supporting information Figures S3 and S4. The calculation was as follows.

$${}^{i}I = \sum_{j=1}^{n} ({}^{j}V_{SW} \times {}^{j}ex{}^{i}Ra) \quad (2)$$

where ${}^{i}I$ is the excess ^{226}Ra or ^{228}Ra inventory, n is the number of box, V_{SW} represents the water volume (m^3) of the surface mixed layer in the study region. The water volume in each triangle was calculated by multiplying the area of the triangle and the average depth of the mixed layer. The integration of water volume over all the triangles was $V_{SW.}$ ${}^{j}V_{SW}$ denotes the water volume of triangle box j. ${}^{j}ex{}^{i}Ra$ represents the average excess ^{226}Ra or ^{228}Ra activities in triangle box j.

2.5.2. Calculation of Residence Time

Radium in the shelf water of NSCS and ECS was influenced by mixing with the offshore water, river inputs, inputs from sediment diffusion and resuspension, and SGD. We assume the systems under study were in steady state on a 2–3 week time scale, that is radium additions including radium fluxes from sediment, river, and groundwater are balanced by losses caused by mixing and its radioactive decay. We used the activity ratio of ^{223}Ra and ^{228}Ra to calculate the water residence time on the shelf of northern South China Sea (NSCS) and East China Sea (ECS) for the regions where the water column was well mixed. Thus we adopted the approach of Moore et al. (2006) that considers continuous radium additions from sediments or SGD with the following mathematical equation to estimate the residence time:

$$\tau = \left[F\left(\frac{^{223}Ra}{ex^{228}Ra}\right) - I\left(\frac{^{223}Ra}{ex^{228}Ra}\right)\right] / \left[I\left(\frac{^{223}Ra}{ex^{228}Ra}\right)\right] \lambda_{223} \quad (3)$$

where $ex^{228}Ra$ denotes the measured ^{228}Ra activity in excess of the value in the offshore surface seawater (3.09 dpm 100 L^{-1} in the NSCS and 1.64 dpm 100 L^{-1} in the ECS). We use ^{223}Ra because its half-life is more appropriate to the time scale of mixing and normalize to $ex^{228}Ra$ to eliminate the influence of mixing with offshore seawater. Here λ_{223} is the decay constant for ^{223}Ra; τ is the water residence time; $F\left(\frac{^{223}Ra}{ex^{228}Ra}\right)$ designates the $^{223}Ra/ex^{228}Ra$ activity ratio (AR) in the input water; $I\left(\frac{^{223}Ra}{ex^{228}Ra}\right)$ represents the $^{223}Ra/ex^{228}Ra$ AR in the systems. We take the average $^{223}Ra/ex^{228}Ra$ AR of 0.039 ± 0.025 in the groundwater along the NSCS, and 0.031 ± 0.024 along the ECS as the initial ratio value in the input water and applied in this model. We will justify this approximation by later showing that SGD is the primary source of ^{223}Ra and ^{228}Ra to the study region.

As the surface water encounters areas where the water column was stratified in the NSCS, equation (3) is no longer applicable because the bottom source of new Ra to surface waters is lost. Here we must use an alternate model, which assumes that there is only a single and constant value for the Ra activity of the source region. Also there are no additions or losses of Ra except for mixing and radioactive decay after the water mass leaves the source region (Moore, 2000a). This model can be expressed as:

$$\left[\frac{^{223}Ra}{ex^{228}Ra}\right]_{obs} = \left[\frac{^{223}Ra}{ex^{228}Ra}\right]_{i} e^{-\lambda_{223}\tau} \quad (4)$$

where, $\left[\frac{^{223}Ra}{ex^{228}Ra}\right]_{obs}$ designates the activity ratio measured in water samples in the study region; and $\left[\frac{^{223}Ra}{ex^{228}Ra}\right]_{i}$ represents the initial activity ratio of the radium source. We neglected the decay of ^{228}Ra here due to the relatively small λ_{228}. The average $^{223}Ra/ex^{228}Ra$ AR of 0.008 ± 0.006 in the station E500a, E602 and A6 in the NSCS was applied in this model. Theoretically, ^{224}Ra also can be applied for the water residence time calculation, however, the 3.66 days half-life restricts its application to ~15 days. In this study, the ^{223}Ra-based ages are more appropriate.

2.5.3. Three End-Member Mixing Model

The end-member mixing model has been widely applied in the SGD studies (Moore, 2003, 2006). In this study, the long-lived Ra isotopes and salinity, parameters we consider conservative in the study regions, were applied to set up a three end-member mixing model to determine fractions of water sources. The following equations were set up.

$$f_j + f_O + f_{GW} = 1 \quad (5)$$

$$S_j f_j + S_O f_O + S_{GW} f_{GW} = S_M \quad (6)$$

$$^{i}Ra_j f_j + {}^{i}Ra_O f_O + {}^{i}Ra_{GW} f_{GW} = {}^{i}Ra_M \quad (7)$$

where f is the fraction of water derived from each end-member, S and Ra denote the salinity and radium activities (dpm 100 L^{-1}), subscripts O and GW represent the oceanic and groundwater end-members, respectively. j refers to the Pearl River, MZCC, and Yangtze River end-member based on temperature and salinity distributions in the WPRE, EPRE and ECS, respectively (Figures 1 and 2). M designates the measured value for individual samples and superscript i is 226 or 228. We ignored the decay of ^{226}Ra and ^{228}Ra due to relatively short time scales of mixing, usually tens of days (Liu et al., 2012), in the shelf region. We also ignored any input of Ra from shelf sediments beyond the river mixing zones. These equations were solved for the fractions of each end-member.

$$f_j = \frac{\left(\frac{^{i}Ra_M - {}^{i}Ra_{GW}}{^{i}Ra_O - {}^{i}Ra_{GW}}\right) - \left(\frac{S_M - S_{GW}}{S_O - S_{GW}}\right)}{\left(\frac{^{i}Ra_j - {}^{i}Ra_{GW}}{^{i}Ra_O - {}^{i}Ra_{GW}}\right) - \left(\frac{S_j - S_{GW}}{S_O - S_{GW}}\right)} \quad (8)$$

$$f_O = \frac{\left(\frac{S_M - S_{GW}}{S_j - S_{GW}}\right) - \left(\frac{^{i}Ra_M - {}^{i}Ra_{GW}}{^{i}Ra_j - {}^{i}Ra_{GW}}\right)}{\left(\frac{S_O - S_{GW}}{S_j - S_{GW}}\right) - \left(\frac{^{i}Ra_O - {}^{i}Ra_{GW}}{^{i}Ra_j - {}^{i}Ra_{GW}}\right)} \quad (9)$$

$$f_{GW} = 1 - f_j - f_O \quad (10)$$

The SGD fluxes in our study regions were then calculated using the following equation.

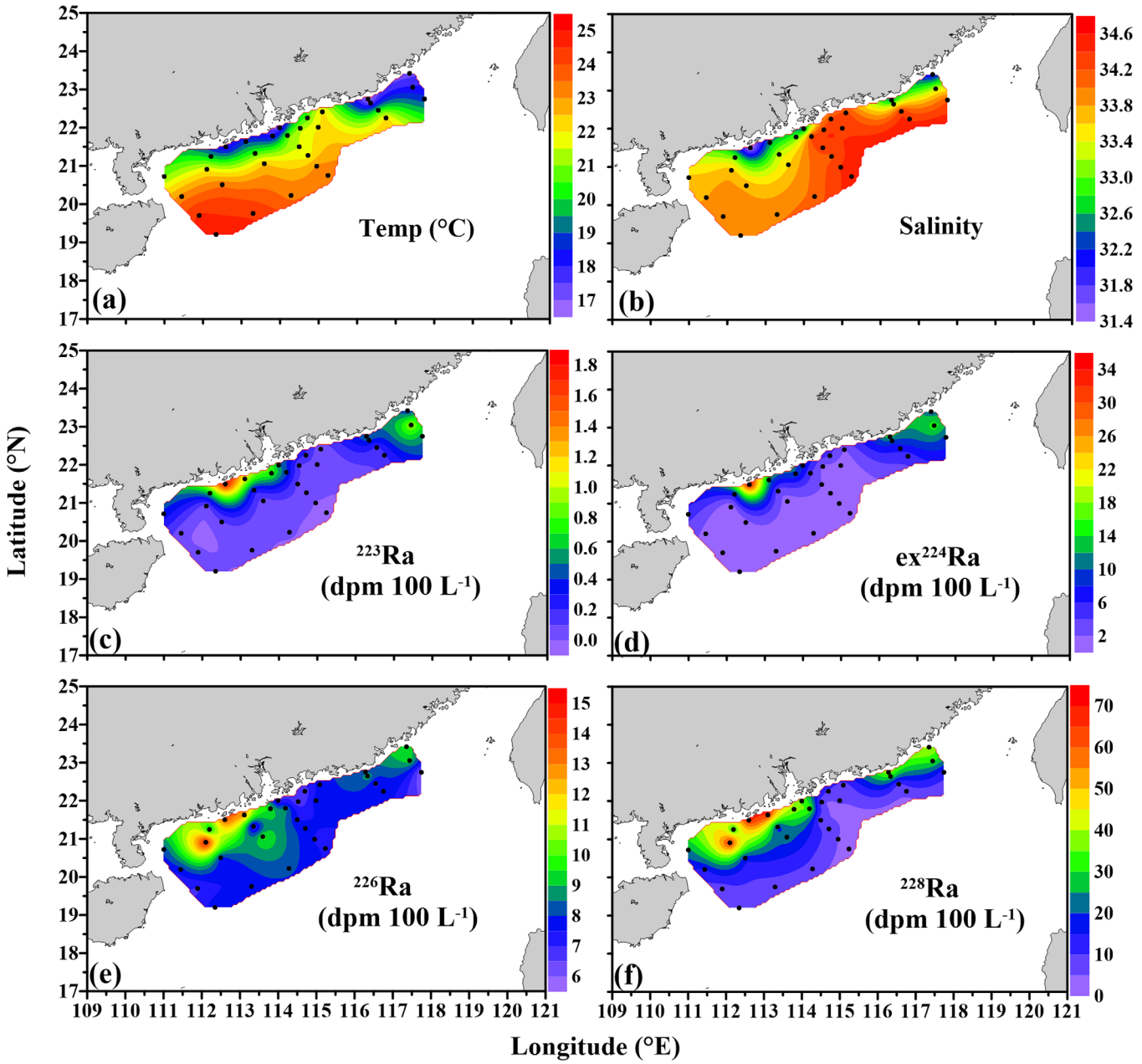

Figure 2. Contour maps showing distributions of (a) temperature (°C), (b) salinity, (c) ^{223}Ra (dpm 100 L^{-1}), (d) ex^{224}Ra (dpm 100 L^{-1}, corrected for the ingrowth from ^{228}Th), (e) ^{226}Ra (dpm 100 L^{-1}) and (f) ^{228}Ra (dpm 100 L^{-1}) on the northern South China Sea shelf during 7–25 January 2010.

$$Q_{sgd} = \frac{f_{GW} \times V_{SW}}{\tau} \tag{11}$$

where Q_{sgd} denotes the flux of submarine groundwater discharge (m^3 d^{-1}), V_{SW} represents the water volume (m^3) of the surface mixed layer in the study region and τ is the residence time.

3. Results

3.1. Hydrography in the NSCS and ECS

As seen from the distributions of temperature and salinity (Figures 2a, 2b, 3a, and 3b), there is a clear signal that large plumes from the Pearl River and Yangtze River, respectively spread southward over the shelf of NSCS and ECS under the intense northeasterly monsoon in winter.

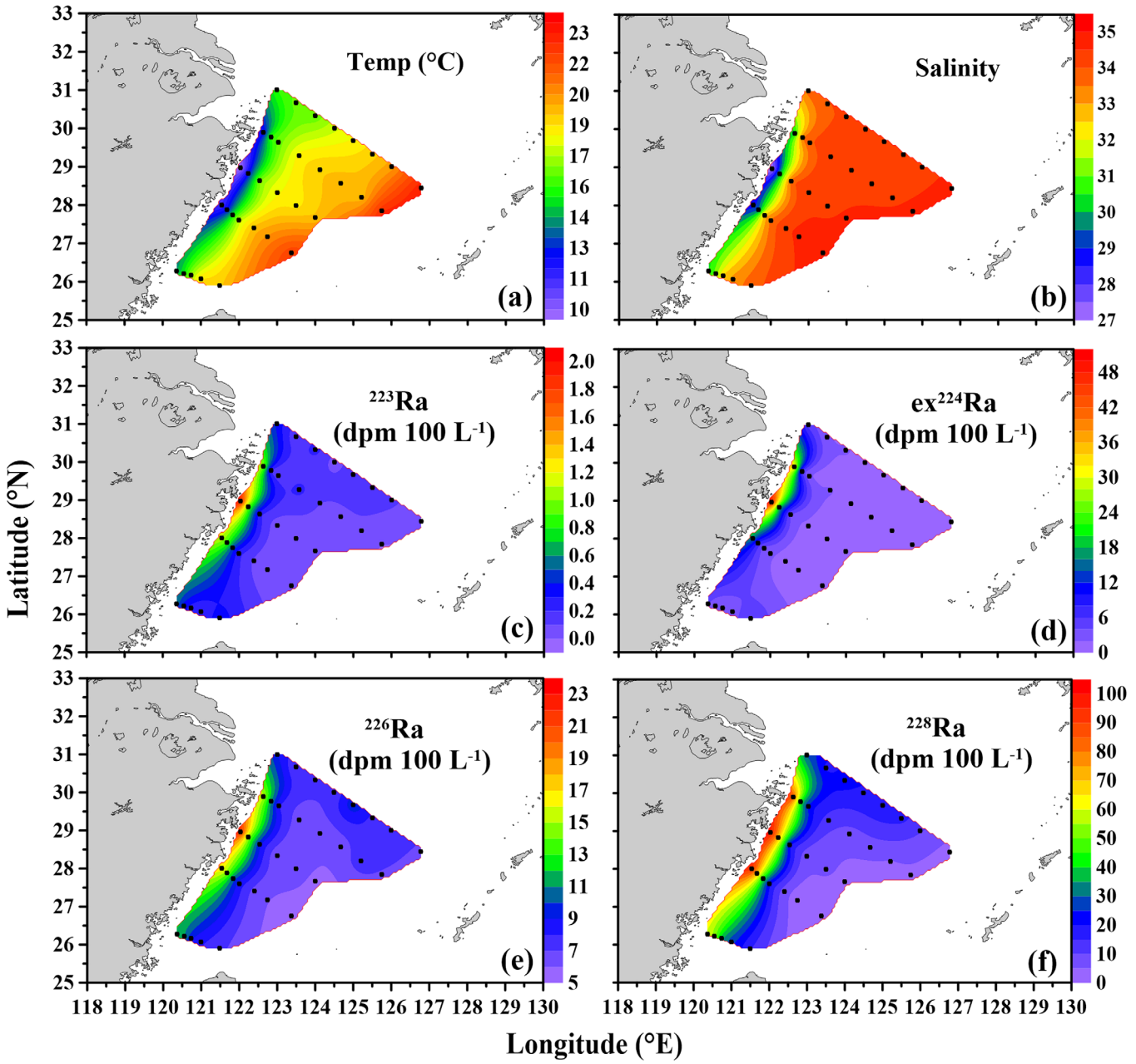

Figure 3. Contour maps showing distributions of (a) temperature (°C), (b) salinity, (c) ^{223}Ra (dpm 100 L^{-1}), (d) ex^{224}Ra (dpm 100 L^{-1}, corrected for the ingrowth from ^{228}Th), (e) ^{226}Ra (dpm 100 L^{-1}) and (f) ^{228}Ra (dpm 100 L^{-1}) on the East China Sea shelf during 24 December 2009 to 4 January 2010.

On the shelf of NSCS, there were two regions characterized by low temperatures (16.8–20.8°C, Figure 2a) and low salinities (31.4–33.3, Figure 2b), one induced by the southward spreading plume from the Pearl River and the other from the Minzhe coastal current (MZCC) driven by the northeasterly monsoon in winter. MZCC, as one of the main current systems on the western side in the Taiwan Strait, emanates from the Yangtze River outlet and Hangzhou Bay. It is composed mainly of the Yangtze River and Qiantangjiang River plumes, incorporating the Oujiang and Minjiang River plumes during its southward spreading. The MZCC occurs in autumn, winter, and spring seasons driven by the northeasterly monsoon: it is characterized by low temperature and low salinity (Pan et al., 2012; Zhang et al., 2005). However, these two regions were separated by a water mass with relatively high temperature (21.2–22.6°C) and salinity (33.9–34.4) offshore surface seawater (Figures 2a and 2b).

Similar scenes emerged on the ECS shelf, where the southward spreading Yangtze River plume was apparent along the ECS coast with low temperatures (9.3–17.4°C, Figure 3a) and salinities (27.1–31.9, Figure 3b). Abundant nutrients from the Yangtze River plume carried by the MZCC lead to increased harmful algal blooms in ECS and Taiwan Strait under strong northeasterly monsoons in dry seasons (Li et al., 2014; Liu et al., 2007). Additionally, we observed a relatively high temperature (18.1–22.9°C, Figure 3a) and salinity (32.3–34.6, Figure 3b) water mass offshore caused by the Taiwan Strait Warm Water and Kuroshio Current Water, both with features of high temperature and salinity.

In addition, based on sectional distributions of temperature, salinity and sigma-t, the water mass in the NSCS was well mixed nearshore and stratified offshore (supporting information Figure S1), while the water column in the ECS was almost well mixed (supporting information Figure S2). The mixed layer depth of each station was estimated from sigma-t profiles in the NSCS and ECS (supporting information Figures S3 and S4). The sigma-t distribution in Transect 6 on NSCS shelf showed a band of low density water nearshore with increasing density offshore, but then the trend reversed with lower density water beyond station S402a, and at station S403 the density was as low as the nearshore water (supporting information Figure S1). This sigma-t anomaly was caused by the low temperature and low salinity water mass from MZCC driven by the northeasterly monsoon in winter (Liu et al., 2007). Similarly, the low density water nearshore and offshore in transect 4 on the ECS shelf were mainly controlled by the low salinity water nearshore and high temperature water offshore, respectively (supporting information Figure S2). However, the high density water mass nearshore in transect 5 on the ECS shelf was caused by the Yangtze River plume with low temperature (supporting information Figure S2).

3.2. Ra Isotopes Distributions on the Shelf of NSCS and ECS

3.2.1. Surface Distributions of Ra Isotopes on the NSCS Shelf

Distributions of surface Ra showed considerable spatial variations in the study region (Figures 2c–2f and supporting information Data Set S1). ^{223}Ra, ex^{224}Ra, ^{226}Ra and ^{228}Ra ranged from 0 to 1.8, 0.4 to 33.8, 6.6 to 14.9, and 3.1 to 67.1 dpm 100 L^{-1}, respectively (Figure 2). The distributions of the four Ra isotopes followed a similar pattern of decreasing gradually with distance offshore due to decay and mixing with offshore seawater. The same pattern was observed in other areas, such as South Atlantic Bight (Moore, 1998, 2000b) and Sicily (Moore, 2006).

The activity of Ra was relatively high in EPRE, which was mainly influenced by MZCC. The activities of ^{223}Ra, ex^{224}Ra, ^{226}Ra and ^{228}Ra ranged from 0.4 to 1.0, 10.4 to 15.4, 6.0 to 9.3, and 31.6 to 40.1 dpm 100 L^{-1}, respectively (Figures 2c–2f). Additionally, there were higher Ra activities in the Pearl River plume, which matched the lower temperature and salinity region (Figures 2a and 2b). The activities of ^{223}Ra, ex^{224}Ra, ^{226}Ra and ^{228}Ra at Station A9, the closest station to the Pearl River Estuary at a water depth of 34 m, were 0.5 ± 0.1, 8.2 ± 0.4, 6.7 ± 0.4, and 33.7 ± 1.3 dpm 100 L^{-1}, respectively (supporting information Data Set S1). Nevertheless, the highest Ra activity (in dpm 100 L^{-1}) appeared at Station F00b, 1.8 for ^{223}Ra, 33.8 for ^{224}Ra, 13.6 for ^{226}Ra and 67.1 for ^{228}Ra, which was 155 km away from Station A9 and coincided with the lower temperature and salinity center of the plume.

3.2.2. Surface Distributions of Ra Isotopes on the ECS Shelf

The distributions of Ra isotopes on the ECS shelf followed a similar distribution pattern to that on the NSCS shelf (Figures 3c–3f and supporting information Data Set S1). Activities of ^{223}Ra, ex^{224}Ra, ^{226}Ra and ^{228}Ra ranged from 0.2 to 1.9, 0.4 to 49.25, 5.5 to 22.1, and 1.6 to 133.5 dpm 100 L^{-1}, respectively. The station with the highest Ra activities did not appear at the Yangtze River mouth, but at Station DH21, which was 245 km away from the Yangtze River mouth, with 1.9 ± 0.4 dpm 100 L^{-1} for ^{223}Ra, 49.2 ± 1.6 dpm 100 L^{-1} for ex^{224}Ra, 22.0 ± 2.7 dpm 100 L^{-1} for ^{226}Ra, and 96.8 ± 4.6 dpm 100 L^{-1} for ^{228}Ra. We suspected that the high Ra activities were the evidence of SGD. However, high activities of ^{226}Ra and ^{228}Ra were not limited to Station DH21, but more widely distributed compared to those of ^{223}Ra and ex^{224}Ra, due to relatively long half-lives of ^{226}Ra and ^{228}Ra.

3.3. Ra Isotopes and Other Dissolved Constituents in the NSCS and ECS Coastal Groundwater

The salinity in the NSCS and ECS coastal groundwater ranged from 0 to 29.8, including fresh groundwater from wells (0–0.7) and brackish groundwater (8.5–29.8) as pore water within the beach sediments (supporting information Figures S5 and S6). Generally speaking, Ra isotopes were enriched in all of the groundwater samples (supporting information Data Sets S2 and S3), with an average of 43 ± 12, 921 ± 302, 108 ± 82 and

490 ± 257 dpm 100 L^{-1} for ^{223}Ra, ex^{224}Ra, ^{226}Ra and ^{228}Ra in the NSCS coastal groundwater, respectively. In the ECS coastal groundwater, the average values for ^{223}Ra, ex^{224}Ra, ^{226}Ra and ^{228}Ra were 0.6 ± 12.4, 949 ± 324, 97 ± 71 and 544 ± 193 dpm 100 L^{-1}, respectively. The errors are one standard deviation, indicating large spatial variability in the activity of Ra in groundwater.

The groundwater also contained high concentrations of nutrients, DIC and TA (supporting information Data Set S2 and S3). However, the concentrations of DIN, DSi, SRP, DIC and TA in the coastal groundwater showed huge spatial variability, with values in the NSCS coastal groundwater of 0.4–1,250, 0.1–20, 30–700, 1,724–13,000 and 1,645–14,200 μM, respectively. Similarly high concentrations were present for these solutes in the ECS coastal groundwater, with values of 13–433, 0.1–12, 27–492, 700-14,000 and 534–13,000 μM, respectively.

4. Discussion

4.1. Water Residence Time

In aquatic systems, the fate of dissolved materials delivered into estuaries and other coastal ecosystems is strongly influenced by residence time. Recently, radium isotopes have been widely used as geochemical tracers to determine the residence time of water masses and ocean circulation (Knee et al., 2011; Moore, 2000a; Moore & de Oliveira, 2008; Street et al., 2008). We used the flux ratio of ^{223}Ra/^{228}Ra to calculate the residence time on the shelf of NSCS and ECS. Based on equations (3) and (4), residence time thus determined ranged from 3 to 48 days on the NSCS shelf and 7 to 47 days on the ECS shelf. On average, the residence time was 18 ± 8 days in WPRE, 19 ± 14 days in EPRE on the NSCS shelf, and 23 ± 10 days on the ECS shelf. These high standard deviations are due to the spatial variations in the study areas (Moore & Krest, 2004).

4.2. Submarine Groundwater Discharge

The relationships between radium isotopes and salinity can be applied to further examine different Ra sources. As shown in supporting information Figures S5 and S6, there were remarkable Ra additions with regard to the conservative mixing line between the river and seawater end-members in our study regions. The addition, however, was not apparent for ex^{224}Ra in the shelf water, probably due to its faster decay (days vs. years) during mixing compared with other Ra isotopes. The excess Ra isotopes can be contributed by SGD and diffusion from sediments in nearshore regions where the water column is well mixed, but not at offshore stations where water is stratified. ^{226}Ra and ^{228}Ra have long half-lives and behaved conservatively on the shelf. Moreover, they were enriched in groundwater relative to the river plume and offshore seawater. Therefore, long-lived Ra isotopes may be used as tracers to estimate the SGD flux. The model established two boxes, one for WPRE and the other for EPRE, to calculate the SGD flux using the three end-member mixing model and the Ra box model in the NSCS.

4.2.1. SGD Fluxes Derived From Three End-Member Mixing Model

It was clear from the salinity versus long-lived Ra plots in the NSCS (Figures 4a–4d) that most of the surface data could be explained by mixing of three end-members, namely Pearl River plume (PRP), offshore surface water (OSW), and SGD in the WPRE, and Min-Zhe coastal current water (MZCCW), OSW, and SGD in the EPRE. The Pearl River plume was not considered in the EPRE because the river plume is deflected southward in winter. Similarly, a three end-member mixing model was established in ECS, with three potential end-members, Yangtze River plume (YRP), offshore surface water (OSW), and SGD (Figures 4e and 4f). End-member values for the Yangtze River water were from literature (Su et al., 2015). The value for the SGD end-member is the mean value in groundwater samples, assuming the beach groundwater represents the composition of all SGD entering the near-shore waters. The values of ^{226}Ra, ^{228}Ra, and salinity for the three end-members applied on the NSCS and ECS shelf were listed in Table 1.

The model results are shown in Figure 5. The fraction of SGD in WPRE on the NSCS shelf ranged from 0.5 to 11.7% (average 2.1 ± 2.5%) based on the ^{226}Ra-salinity mixing model and 0.3 to 14.4% (average 2.9 ± 3.1%) using the ^{228}Ra-salinity relationship. Meanwhile, the groundwater fraction in EPRE ranged from 0.1 to 3.8% (average 1.2 ± 1.2%) and 0.1 to 9.7% (average 1.9 ± 2.5%), respectively. In addition, the fraction of groundwater on the ECS shelf based on ^{226}Ra-S and ^{228}Ra-S mixing model ranged from 1.8 to 8.2% (average 3.9 ± 1.5%) and 0.3 to 12.5% (average 3.9 ± 3.6%), respectively.

Based on equation (11) and values of parameters in Table 2, the SGD fluxes were calculated to be 1.6–38 × 10^9 m^3 d^{-1} using ^{226}Ra and 10–47 × 10^9 m^3 d^{-1} using ^{228}Ra in WPRE, and 0.2–4.3 × 10^9 m^3 d^{-1} based on

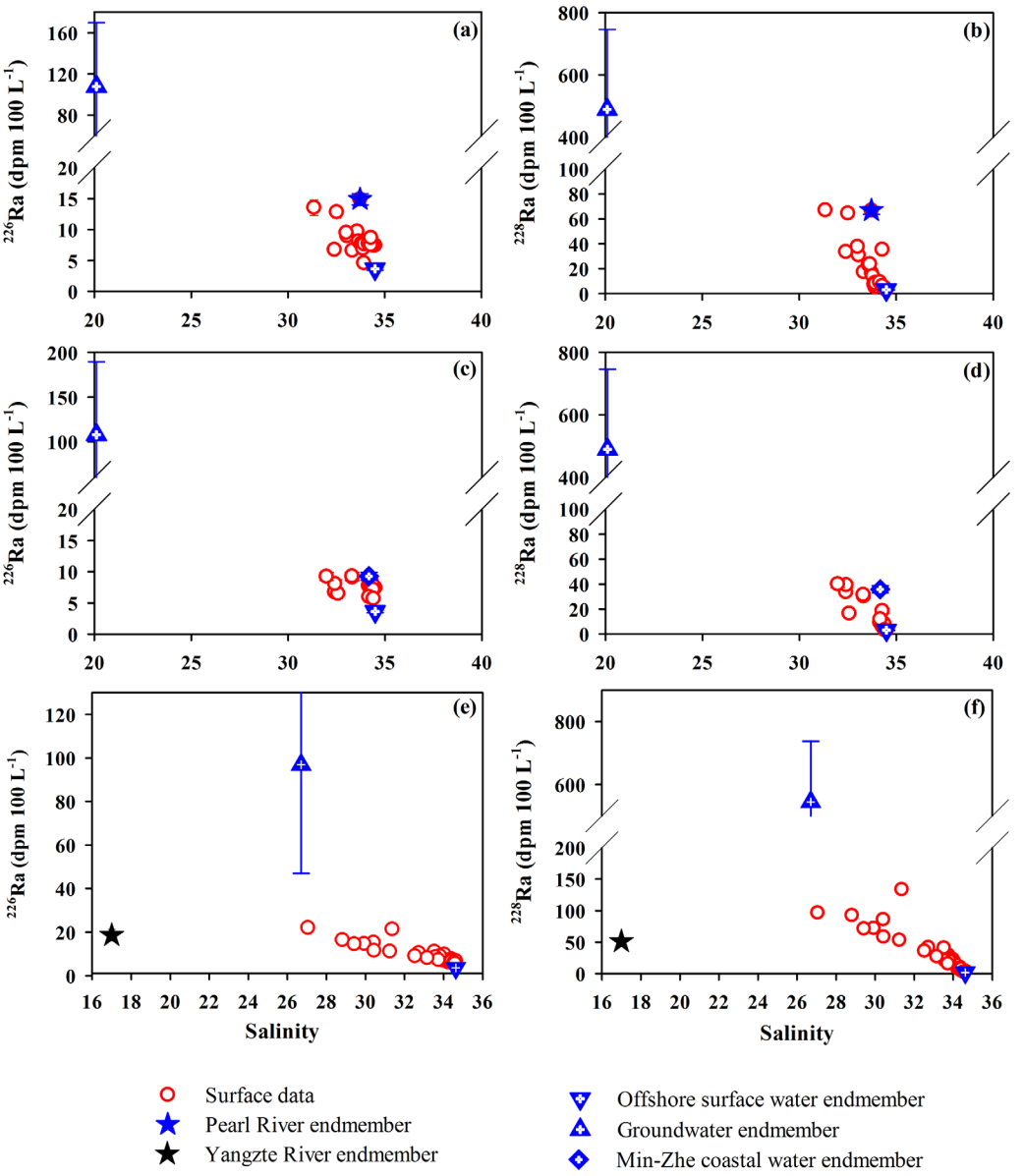

Figure 4. Salinity versus ^{226}Ra and ^{228}Ra in the surface water of WPRE (a and b) and EPRE (c and d) on the northern South China Sea shelf and East China Sea shelf (e and f). Error bars reflect the spatial variation (1σ).

^{226}Ra and 0.2–11 $\times$ 10^{9} m^{3} d^{-1} based on ^{228}Ra in EPRE. In the same way, the SGD fluxes on the ECS shelf were 9.8–46 $\times$ 10^{9} and 1.5–70 $\times$ 10^{9} m^{3} d^{-1}, respectively.

4.2.2. SGD Fluxes Estimated Using Box Models

In addition, box models were used to quantify the SGD input based on equation (1) and values of parameters listed in Table 2. Primarily, the total offshore ^{226}Ra and ^{228}Ra fluxes were obtained using the excess ^{226}Ra and ^{228}Ra inventory divided by residence time in the study area. Here, based on equation (2) and the residence time, the ^{226}Ra fluxes in the WPRE, EPRE, and ECS were calculated to be 2.6–5.6 $\times$ 10^{12}, 0.4–2.9 $\times$ 10^{12} and 4.3–11 $\times$ 10^{12} dpm d^{-1}, respectively. The ^{228}Ra fluxes were 1.7–3.9 $\times$ 10^{13}, 0.3–1.9 $\times$ 10^{13} and 2.7–6.9 $\times$ 10^{13} dpm d^{-1}, respectively.

The riverine sources of Ra include the dissolved Ra and Ra that desorbs from particulate matter. The dissolved flux was calculated by multiplying the river flow rate with the river Ra activity. The Ra activities in the Pearl River (Wang, 2014) and Yangtze River (Su et al., 2015) were the sum of the dissolved Ra and 40% of the Ra carried in suspension at the river mouth (Gu et al., 2012). The riverine ^{226}Ra flux was calculated to be

Table 1
End-Member Values Used for ^{226}Ra-S, and ^{228}Ra-S Three End-Member Mixing Model to Estimate Submarine Groundwater Discharge Fluxes to the Northern South China Sea (WPRE and EPRE) Shelf and East China Sea Shelf

	^{226}Ra dpm 100 L^{-1}	^{228}Ra dpm 100 L^{-1}	Salinity	References
WPRE and EPRE				
Offshore surface water	6.0 ± 0.4	3.1 ± 0.4	34.5	This study
Groundwater	107.8 ± 81.9	489.6 ± 256.8	20.1	This study
Pearl river plume[a]	14.9 ± 0.9	66.9 ± 3.1	33.7	This study
Min-Zhe coastal current water[b]	9.3 ± 0.6	35.9 ± 2.4	34.2	This study
East China Sea				
Offshore surface water	5.6 ± 0.1	1.6 ± 0.1	34.6	This study
Groundwater	96.9 ± 71.0	544.5 ± 193.2	26.7	This study
Yangtze river water	18.6 ± 0.2	51.1 ± 2.7	17.0	Su et al. (2015)

Note. "±" indicates one standard deviation.
[a]Endmember in WPRE. [b]Endmember in EPRE.

2.3×10^{11} and 6.5×10^{11} dpm d^{-1}, accounting for 6.6% and 8.5% of the total ^{226}Ra flux to the WPRE and ECS box model, respectively. Similarly, the riverine ^{228}Ra flux was 4.4×10^{11} and 9.3×10^{11} dpm d^{-1},

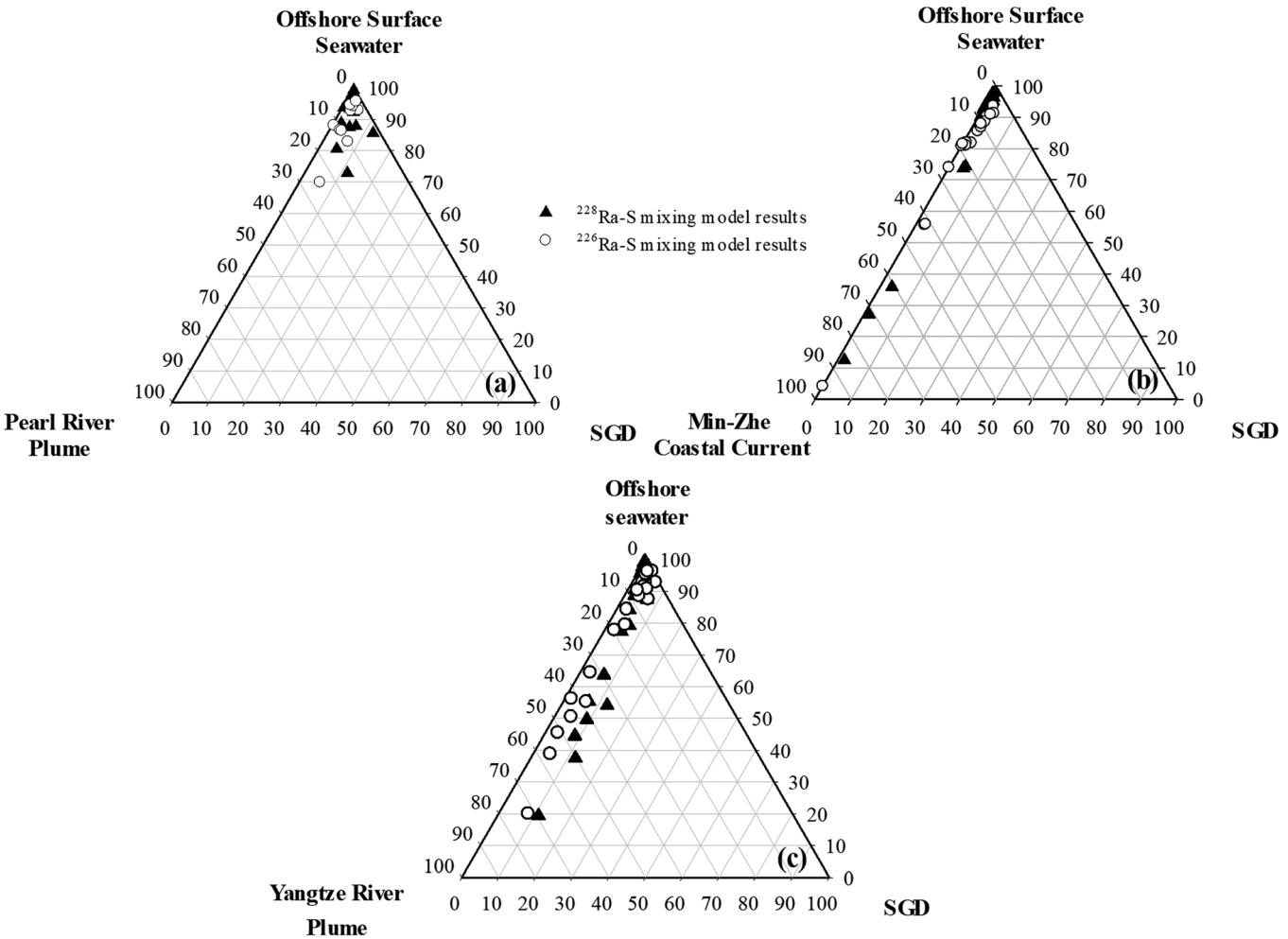

Figure 5. Ternary diagram illustrating percentage contributions from each endmember for surface water of the northern South China Sea (a for WPRE and b for EPRE), and East China Sea (c) based on Ra and salinity mixing model.

Table 2
Values of Parameters Applied to Estimate Submarine Groundwater Discharge Fluxes to the Northern South China Sea and East China Sea Shelf

Parameters	NSCS		ECS		Units
	^{226}Ra	^{228}Ra	^{226}Ra	^{228}Ra	
Ra_{riv}	78.9 ± 1.6	150.8 ± 4.7	62.1 ± 2.5	89.2 ± 4.7	dpm 100 L^{-1}
Ra_{sgd}	107.8 ± 81.9	489.6 ± 256.8	96.9 ± 71.0	544.5 ± 193.2	dpm 100 L^{-1}
Q_{riv}	2.9×10^8		1.1×10^9		m^3 d^{-1}
τ (Residence time)	18 ± 8[a]		23 ± 10		days
	19 ± 14[b]				
A_{sed}	3.9×10^{10a}		1.6×10^{11}		m^2
	3.2×10^{10b}				
V_{SW}	5.9×10^{3a}		1.3×10^4		km^3
	2.2×10^{3b}				

Note. "±" indicates one standard deviation.
[a]Residence time, sediment area and water volume in EPRE. [b]Residence time, sediment area and water volume in WPRE.

accounting for 1.9% in both cases. Note that the Ra from the Pearl River plume did not influence the EPRE due to the southward flow of the river plume.

An additional source of Ra is its release from benthic sediments due to diffusion, bioturbation, and irrigation. This source can be calculated by multiplying the area of the region where the mixed layer extends to the bottom with the Ra flux from the sediments. We assume that the sediments are in steady state so the rate of Ra regeneration within the upper sediments equals its flux out of the sediment. Coarser-grained (sandy) sediments cover approximately 50% and 60% of the NSCS and ECS while the remaining is fine-grained (mud) sediments (Niino & Emery, 1961). We used the regeneration rate of 31.42 and 0.63 dpm m^2 d^{-1} for ^{228}Ra from fine-grained and coarser-grained sediments, respectively (Moore et al., 2008). For ^{226}Ra we used the global average regeneration rate of 0.45 dpm m^2 d^{-1} for ^{226}Ra in continental shelf sediment (Hancock et al., 2000; Liu et al., 2014). The ^{226}Ra flux from benthic sediments diffusion account for only 0.5% (1.8×10^{10} dpm d^{-1}), 0.09% (1.4×10^{10} dpm d^{-1}), and 0.9% (7.0×10^{10} dpm d^{-1}) of the total ^{226}Ra flux to the WPRE, EPRE, and ECS shelf, respectively. The percentage of ^{228}Ra flux contributed from benthic sediments accounted for 2.7% (6.3×10^{11} dpm d^{-1}), 4.5% (5.0×10^{11} dpm d^{-1}), and 4.2% (2.0×10^{12} dpm d^{-1}), respectively.

The Ra flux derived from alongshore transport can be a source or sink of Ra. This is determined by the speed and direction of the current at the two boundaries perpendicular to the coast, and the difference of the Ra activities between the two boundaries. The current in the NSCS in winter was southward with the surface velocity ranging from 0.01 to 0.23 m s^{-1} (Gan & Qu, 2008), and an average rate of 0.13 m s^{-1}. The water transport flux was calculated by multiplying the water velocity and the cross-sectional area, and then the difference of water transport flux between two sections was the net water transport flux in the study region. Thus, the net water transport flux in the WPRE was 5.3×10^{10} m^3 d^{-1}. The difference in ^{226}Ra and ^{228}Ra activities were 0.6 and 16.3 dpm m^{-3}, respectively. Thus the ^{226}Ra and ^{228}Ra fluxes produced by alongshore transport were estimated to be -3.1×10^{10} and 8.7×10^{11} dpm d^{-1}, only 0.9% and 3.8% of the total ^{226}Ra and ^{228}Ra fluxes in the WPRE, respectively. It must be noted that the negative and positive number mean a Ra sink and source for the box model, respectively. Similarly, for the EPRE, the water net transport flux was 3.6×10^{10} m^3 d^{-1}, and the ^{226}Ra and ^{228}Ra activities in the southern border were 0.36 and 0.54 dpm m^{-3} higher than that in the northern border, respectively. Compared to the total Ra flux, the alongshore transport provided about 0.8% (-1.3×10^{10} dpm d^{-1}) and 0.2% (-2.0×10^{10} dpm d^{-1}) for ^{226}Ra and ^{228}Ra flux. Similarly, we did the calculation for the ECS shelf. Liu and Gan (2012) showed that the dominant current direction was southward with an average speed of 0.14 m s^{-1} within the 200 m isobath. This produced a net transport flux of 1.4×10^{11} m^3 d^{-1}, and the Ra activities in the southern boundary was relatively high compared to the northern boundary with ^{226}Ra and ^{228}Ra of 0.4 and 15.6 dpm m^{-3}, respectively. Similarly, the ^{226}Ra and ^{228}Ra flux contributed by current were estimated to be -5.7×10^{10} dpm d^{-1} and -2.2×10^{12} dpm d^{-1}, accounting for 0.7% and 4.5% of the total Ra flux, respectively.

In summary, the total Ra inputs to the study regions from rivers and sediment diffusion accounted for several percent of the total Ra budget (supporting information Table S2). Thus, the input from SGD was the

Table 3
The Synthesis of SGD Fluxes (10^9 m^3 d^{-1}) Calculated by Two Models in the Study Areas

	Calculation models			
	Three end-member mixing model		Box model	
Study areas	^{226}Ra	^{228}Ra	^{226}Ra	^{228}Ra
WPRE	1.6–38	10–47	0.1–6.1	0.7–7.9
EPRE	0.2–4.3	0.2–11	0.1–3.2	0.1–4.2
ECS	9.8–46	1.5–70	0.9–14	3.7–14

most important Ra source (more than 90%), lending support to the assumption in calculating the residence time. Finally, based on equation (1), the total SGD fluxes derived from the ^{226}Ra box model were 0.1–6.1 × 10^9, 0.1–3.2 × 10^9 and 0.9–13.5 × 10^9 m^3 d^{-1} on the WPRE, EPRE and ECS shelf, respectively; and for the ^{228}Ra box model, the SGD fluxes were similarly 0.7–7.9 × 10^9, 0.1–4.2 × 10^9 and 3.7–13.7 × 10^9 m^3 d^{-1} on the WPRE, EPRE, and ECS shelf, respectively.

The results of SGD using the two models were synthesized in Table 3. We found that the SGD fluxes calculated by the three end-member mixing model were larger than the results obtained using the box model. In the box model, we considered almost all of Ra sources to the study area, including groundwater input, river input, benthic sediments diffusion and alongshore transport. However, only three end-members (groundwater, offshore seawater and river input) were included in the three end-member mixing model, possibly leading to the overestimation of the fraction of groundwater end-member, and consequent higher SGD fluxes. Considering the large ranges in the SGD flux estimates (Table 3), we thus used the SGD fluxes calculated taking the average values of each parameter in the three end-member mixing models and box models to represent the SGD fluxes in our study regions. The SGD fluxes were estimated to be 3.8–9.5 × 10^9 m^3 d^{-1} in WPRE, 1.4–2.2 × 10^9 m^3 d^{-1} in EPRE and 0.7–2.2 × 10^{10} m^3 d^{-1} in ECS. Compared to earlier studies, the SGD in winter was an order of magnitude higher in EPRE (0.2–0.4 × 10^9 m^3 d^{-1}; Liu et al., 2012) and 3x in ECS (0.2–1.0 × 10^9 m^3 d^{-1} in the Changjiang effluent plume; Gu et al., 2012), respectively.

To put these results into context we can scale the fluxes to the shoreline being investigated. The shoreline lengths of the WPRE, EPRE and ECS were 2,314, 2,202, and 3,010 km. When scaled to these coastline lengths, the SGD rates were 1.6–4.1 × 10^3, 0.6–1.0 × 10^3 and 2.4–7.2 × 10^3 m^3 m^{-1} d^{-1} in WPRE, EPRE and ECS, respectively. A comparison of SGD fluxes from various regions is given in Table 4. The fluxes we estimated are larger than the global average SGD flux, but are approximately in the same order of magnitude compared with other studies in the same region (Table 4). The higher value for the ECS shelf may be due to the much larger area of the shallow shelf.

4.3. Biogeochemical Impacts of SGD on the NSCS and ECS Shelf

It should be noted that the SGD fluxes estimated here include fresh groundwater and recirculated seawater that has infiltrated coastal or permeable sediments on the shelf. The average net annual groundwater recharge rates into groundwater system along the shorelines of WPRE, EPRE and ECS shelf were 1.3 × 10^8 m^3 d^{-1}, 8.7 × 10^7 m^3 d^{-1} and 5.5 × 10^7 m^3 d^{-1} (Zhang et al., 2005). These only account for approximately 4.1%, 6.2% and 0.75% of the SGD fluxes, respectively. Thus our calculated SGD fluxes are composed mainly

Table 4
A Comparison of SGD Fluxes at Various Regions

Regions	Date	Coast length (km)	SGD fluxes (10^3 m^3 m^{-1} d^{-1})	References
Yangtze Estuary, China	Aug 2009	320	0.6–3.1	Gu et al. (2012)
Northern South China Sea	Jul 2008	308	1.1–1.2	Liu et al. (2012)
Yeongil Bay, Korea	Aug 2004	57	0.1	Kim et al. (2007)
Mansan Bay, Korea	Aug 2006	72	0.08	Lee et al. (2009)
Sicily	Jul 2001	150	1	Moore, (2006)
Southwest Florida Shelf, USA	Oct 2009	350	0.5	Liu et al. (2014)
South Atlantic Bight, USA	Jul-1994 to Feb 2000	320–600	0.6–1.3	Moore, (2010b)
Southwest Brazil	Dec 2004	240	0.35	Windom et al., (2006)
Mediterranean	1981–2014	64,000	0.01–0.21	Rodellas et al., (2015)
Atlantic	1981–1999	85,000	0.65–1.3	Moore et al., (2008)
Global	1971–2014	13,64,700	0.24	Kwon et al. (2014)
WPRE	Jan 2010	2,314	1.6–4.1	This study
EPRE	Jan 2010	2,202	0.6–1.0	This study
ECS	Dec 2009	3,010	2.4–7.2	This study

Table 5
SGD-Associated Nutrients (DIN, SRP, and DSi), Dissolved Inorganic Carbon (DIC), and Total Alkalinity (TA) Fluxes and the Linear Shore Normalized Fluxes into the Northern South China Sea Shelf and East China Sea Shelf

		Northern South China Sea		
Fluxes	Units	WPRE	EPRE	East China Sea
DIN	mol d^{-1}	0.4–1.1 × 10^9	1.6–2.5 × 10^8	0.9–2.7 × 10^9
	mol m^{-1} d^{-1}	0.5–1.2 × 10^3	0.2–0.4 × 10^3	0.8–2.4 × 10^3
SRP	mol d^{-1}	1.7–4.3 × 10^6	0.9–1.3 × 10^6	3.6–10.9 × 10^6
	mol m^{-1} d^{-1}	1.9–4.7	1.2–1.9	3.2–9.8
DSi	mol d^{-1}	0.6–1.6 × 10^9	2.4–3.7 × 10^8	1.3–3.8 × 10^9
	mol m^{-1} d^{-1}	0.7–1.7 × 10^3	0.4–0.5 × 10^3	1.1–3.4 × 10^3
DIC	mol d^{-1}	1.0–2.6 × 10^{10}	3.8–5.9 × 10^9	1.9–5.6 × 10^{10}
	mol m^{-1} d^{-1}	1.1–2.8 × 10^4	0.6–0.9 × 10^4	1.7–5.1 × 10^4
TA	mol d^{-1}	1.0–2.4 × 10^{10}	3.6–5.5 × 10^9	1.8–5.4 × 10^{10}
	mol m^{-1} d^{-1}	1.1–2.7 × 10^4	0.5–0.8 × 10^4	1.6–4.8 × 10^4

of recirculated seawater. Therefore, the nutrients, DIC and TA fluxes carried by SGD can be calculated by multiplying the SGD flux with the difference between the average concentrations in saline groundwater and seawater (supporting information Table S3). The nutrient and carbon fluxes and area-normalized fluxes to the NSCS (WPRE and EPRE) and ECS shelf from SGD are listed in Table 5. The shoreline-normalized nutrients, DIC and TA fluxes from SGD into WPRE were a factor of ~2–3 greater than that into EPRE and have a similar magnitude to that in ECS. In addition, it is quite clear that SGD was the dominant inorganic carbon source for the shelf water in NSCS and ECS compared with the carbon fluxes from local major rivers, the dry season flux from the Pearl River (6.5 × 10^8 mol d^{-1}) (Guo et al., 2008) and the annual flux from the Yangtze River (4.2 × 10^9 mol d^{-1}) (Zhai et al., 2007).

According to the volume and residence time of our study areas, when the DIC flux derived from SGD was released to seawater, the DIC concentrations in the seawater would increase by 31–77, 33–50, and 32–98 μM, and account for 1.5–3.8%, 1.6–2.5% and 1.6–4.9% of the average DIC concentration on the WPRE, EPRE and ECS shelves, respectively. The shelf scale SGD is a significant net source of nutrients and carbon to the study regions, and it likely has great impacts on the local marine ecosystem when such abundant nutrients and carbon are delivered into the upper water column. Shelf-scale SGD cannot be overlooked in shelf biogeochemical studies considering their wide occurrences and important net export material fluxes into shelf waters. In studies of biogeochemistry, especially the carbon cycle in marginal seas, the role of SGD on the carbon budget in regional and global scales must be considered.

4.4. Uncertainty Analysis

Based on error propagation (supporting information Methods), the major uncertainty in the SGD flux estimated using the three end-member mixing model comes from the spatial variation in the fraction of SGD, accounting for 78.8–81.9%, 89.9–95.5% and 64.3–80.1%, respectively (supporting information Table S4). However, the uncertainty in the fraction of SGD mainly resulted from the spatial variation of the SGD endmember. If the offshore SGD endmembers were 50% different from the coastal groundwater, the SGD estimates would change by 27.3% for ^{226}Ra and 36.9% for ^{228}Ra in the WPRE, 38.7% for ^{226}Ra and 44.4% for ^{228}Ra in the EPRE, 35.2% for ^{226}Ra and 37.4% for ^{228}Ra in the ECS, respectively, indicating the importance to evaluate the groundwater endmember accurately. The residence time was a minor error source, which accounted for 18.1–21.2%, 4.5–10.1% and 19.9–35.7% uncertainty in WPRE, EPRE and ECS, respectively (supporting information Table S4).

The uncertainty in the SGD flux based on the box model was estimated to be mainly from spatial variation in the residence time (38.7–58.4%, 25.9–45.5% and 49.1–82.1% uncertainty in WPRE, EPRE and ECS, respectively), and the spatial variation in Ra activity in the coastal groundwater (41.6–61.2%, 54.4–73.9% and 17.9–50.9% uncertainty in WPRE, EPRE and ECS, respectively). The uncertainties in the inventory of Ra in the study region and the Ra activity in the river endmember were insignificant since the contribution to total uncertainties were less than 1% (supporting information Table S5). Here the uncertainty in Q_{riv}, A_{sed} and F_{sed} was taken to be 0.

The uncertainty in the net SGD-associated nutrients and carbon fluxes resulted not only from the uncertainty in the SGD flux, but also from the spatial variation in the concentration of these materials in the

coastal groundwater and seawater. The uncertainties caused by SGD flux and the nutrients concentration in coastal groundwater were nearly in the same magnitude, however, the spatial variation in the concentration of these materials in coastal groundwater was a more significant error source (the contribution to total uncertainty for carbon and nutrients varied from 65.0 to 80.2%, from 60.9 to 78.2% and from 62.2 to 90.9% in WPRE, EPRE and ECS, respectively) in this study (supporting information Table S6). The uncertainty resulting from the spatial variation in the concentration of materials in seawater was insignificant (the uncertainties were less than 0.3%), except for the SRP flux, which resulted in 13.7%, 6.9% and 3.6% uncertainty in WPRE, EPRE and ECS, respectively (supporting information Table S6). Even considering these uncertainties, the conclusions drawn using the average values of the parameters in this study would not change.

5. Conclusions

We calculated the SGD fluxes to the NSCS and ECS shelf in winter combining the three end-member mixing model with the Ra box model. Notably, both the fresh groundwater and circulated seawater that has infiltrated coastal or permeable sediments on the shelf were contained in the SGD fluxes estimated here. SGD fluxes on NSCS (west and east of the Pearl River Estuary, WPRE and EPRE, respectively) and ECS shelf in winter were estimated to be 3.8–9.5 $\times$ 10^9, 1.4–2.2 $\times$ 10^9 and 0.7–2.2 $\times 10^{10}$ m^3 d^{-1}, respectively. Our results were equivalent to the SGD flux to the entire Mediterranean Sea, and were an order of magnitude greater than fluxes to the South Atlantic Bight. SGD associated nutrient fluxes into WPRE, EPRE and ECS were almost in the same order of magnitude, 0.2–2.4 $\times$ 10^3 mol m^{-1} d^{-1} for DIN, 1.2–9.8 mol m^{-1} d^{-1} for SRP, and 0.4–3.4 $\times$ 10^3 mol m^{-1} d^{-1} for DSi. Moreover, SGD delivered 1.1–2.8 $\times$ 10^4, 0.6–0.9 $\times$ 10^4, 1.7–5.1 $\times$ 10^4 mol m^{-1} d^{-1} DIC and 1.1–2.7 $\times$ 10^4, 0.5–0.8 $\times$ 10^4, 1.6–4.8 $\times$ 10^4 mol m^{-1} d^{-1} TA to WPRE, EPRE and ECS, respectively. As a result, the DIC concentrations in seawater would increase by tens of micromoles per liter. We found that the shelf-scale SGD is an important carbon source and can have great impacts on the carbonate system. Although there still exist many difficulties and uncertainties in studying SGD on shelf scale, the influences of SGD in coastal and shelf-scale ocean cannot be ignored. In future studies of biogeochemistry, especially the carbon cycle, the role of SGD on the carbon budget in regional and global scales should be considered.

Acknowledgments
We thank the crew on R/V Dongfanghong II for their assistance in the shelf cruises. Shuling Wang and Zhangyong Wang helped in groundwater sampling and measurements. ^{226}Ra and ^{228}Ra on the ECS shelf and some on the NSCS shelf were measured in Chih-An Huh's lab. We appreciate the CTD data from Jianyu Hu. We are grateful to anonymous reviewers for their constructive comments. The cruises were supported by the MOST (2009CB421204) and the sampling was funded by the National Natural Science Foundation of China (41006041). The study was also funded by MOST (2015CB954001) and the National Natural Science Foundation of China (41576074). Readers can find and access all the data from the data sets in the supporting information.

References

Beardsley, R. C., Limeburner, R., Yu, H., & Cannon, G. A. (1985). Discharge of the Changjiang (Yangtze River) into the East China Sea. *Continental Shelf Research*, *4*(1–2), 57–76. https://doi.org/10.1016/0278-4343(85)90022-6

Burnett, W. C., Bokuniewicz, H., Huettel, M., Moore, W. S., & Taniguchi, M. (2003). Groundwater and pore water inputs to the coastal zone. *Biogeochemistry*, *66*(1/2), 3–33. https://doi.org/10.1023/B:BIOG.0000006066.21240.53

Cai, W. J., Dai, M., Wang, Y., Zhai, W., Huang, T., Chen, S., et al. (2004). The biogeochemistry of inorganic carbon and nutrients in the Pearl River estuary and the adjacent Northern South China Sea. *Continental Shelf Research*, *24*(12), 1301–1319. https://doi.org/10.1016/j.csr.2004.04.005

Cai, W. J., & Wang, Y. (1998). The chemistry, fluxes and sources of carbon dioxide in the estuarine waters of the Satilla and Altamaha Rivers, Georgia. *Limnology and Oceanography*, *43*, 657–668. https://doi.org/10.4319/lo.1998.43.4.0657

Charette, M. A., & Buesseler, K. O. (2004). Submarine groundwater discharge of nutrients and copper to an urban subestuary of Chesapeake Bay (Elizabeth River). *Limnology and Oceanography: Methods*, *49*(2), 376–385. https://doi.org/10.4319/lo.2004.49.2.0376

Charette, M. A., Moore, W. S., & Burnett, W. C. (2008). Uranium-and thorium-series nuclides as tracers of submarine groundwater discharge. In J. K. C. S. Krishnaswami (Ed.), *U-Th series Nuclides in Aquatic systems* (p. 440). Oxford, UK: Elsevier.

Dai, M., Wang, L., Guo, X., Zhai, W., Li, Q., He, B., & Kao, S. J. (2008). Nitrification and inorganic nitrogen distribution in a large perturbed river/estuarine system: The Pearl River Estuary, China. *Biogeosciences*, *5*, 1227–1244. https://doi.org/10.5194/bg-5-1227-2008

Dong, L., Su, J., Ah Wong, L., Cao, Z., & Chen, J.-C. (2004). Seasonal variation and dynamics of the Pearl River plume. *Continental Shelf Research*, *24*(16), 1761–1777. https://doi.org/10.1016/j.csr.2004.06.006

Dulaiova, H., Burnett, W. C., Chanton, J. P., Moore, W. S., Bokuniewicz, H. J., Charette, M. A., & Sholkovitz, E. (2006). Assessment of groundwater discharges into West Neck Bay, New York, via natural tracers. *Continental Shelf Research*, *26*(16), 1971–1983. https://doi.org/10.1016/j.csr.2006.07.011

Gan, J., & Qu, T. (2008). Coastal jet separation and associated flow variability in the southwest South China Sea. *Deep Sea Research, Part I: Oceanographic Research Papers*, *55*(1), 1–19.

Garcia-Solsona, E., Garcia-Orellana, J., Masqué, P., Garcés, E., Radakovitch, O., Mayer, A., et al. (2009). An assessment of karstic submarine groundwater and associated nutrient discharge to a Mediterranean coastal area (Balearic Islands, Spain) using radium isotopes. *Biogeochemistry*, *97*(2–3), 211–229. https://doi.org/10.1007/s10533-009-9368-y

Giffin, C., Kaufman, A., & Broecker, W. S. (1963). Delayed coincidence counter for the assay of actinon and thoron. *Journal of Geophysical Research*, *68*(6), 1749–1757. https://doi.org/10.1029/JZ068i006p01749

Gu, H., Moore, W. S., Zhang, L., Du, J., & Zhang, J. (2012). Using radium isotopes to estimate the residence time and the contribution of submarine groundwater discharge (SGD) in the Changjiang effluent plume, East China Sea. *Continental Shelf Research*, *35*, 95–107. https://doi.org/10.1016/j.csr.2012.01.002

Guo, X., Cai, W.-J., Zhai, W., Dai, M., Wang, Y., & Chen, B. (2008). Seasonal variations in the inorganic carbon system in the Pearl River (Zhujiang) estuary. *Continental Shelf Research*, *28*(12), 1424–1434. https://doi.org/10.1016/j.csr.2007.07.011

Han, A., Dai, M., Kao, S.-J., Gan, J., Li, Q., Wang, L., Zhai, W., & Wang, L. (2012). Nutrient dynamics and biological consumption in a large continental shelf system under the influence of both a river plume and coastal upwelling. *Limnology and Oceanography: Methods*, *57*(2), 486–502. https://doi.org/10.4319/lo.2012.57.2.0486

Hancock, G. J., Webster, I. T., Ford, P. W., & Moore, W. S. (2000). Using Ra isotopes to examine transport processes controlling benthic fluxes into a shallow estuarine lagoon. *Geochimica et Cosmochimica Acta*, *64*(21), 3685–3699. https://doi.org/10.1016/S0016-7037(00)00469-5

Hong, Q., Cai, P., Shi, X., Li, Q., & Wang, G. (2016). Solute transport into the Jiulong River estuary via pore water exchange and submarine groundwater discharge: New insights from $^{224}Ra/^{228}Th$ disequilibrium. *Geochimica et Cosmochimica Acta*, *198*, 338–359. https://doi.org/10.1016/j.gca.2016.11.002

Kim, G., Ryu, J. W., & Hwang, D. W. (2007). Radium tracing of submarine groundwater discharge (SGD) and associated nutrient fluxes in a highly-permeable bed coastal zone, Korea. *Marine Chemistry*, *109*(3–4), 307–317. https://doi.org/10.1016/j.marchem.2007.07.002

Knee, K. L., Solsona, E. G., Orellana, J. G., Boehm, A. B., & Paytan, A. (2011). Using radium isotopes to characterize water ages and coastal mixing rates: A sensitivity analysis. *Limnology and Oceanography: Methods*, *9*(9), 380–395. https://doi.org/10.4319/lom.2011.9.380

Kohout, F. A., & Kolipinski, M. C. (1967). Biological zonation related to groundwater discharge along the shore of Biscayne Bay, Miami, Florida. *Chemical Communications*, *51*(82), 15110–15113.

Kwon, E. Y., Kim, G., Primeau, F., Moore, W. S., Cho, H. M., Devries, T., et al. (2014). Global estimate of submarine groundwater discharge based on an observationally constrained radium isotope model. *Geophysical Research Letters*, *41*, 8438–8444. https://doi.org/10.1002/2014GL061574

Lee, H. J., & Chao, S. Y. (2003). A climatological description of circulation in and around the East China Sea. *Deep Sea Research, Part II: Topical Studies in Oceanography*, *50*(6–7), 1065–1084. https://doi.org/10.1016/s0967-0645(03)00010-9

Lee, Y. W., Hwang, D. W., Kim, G., Lee, W. C., & Oh, H. T. (2009). Nutrient inputs from submarine groundwater discharge (SGD) in Masan Bay, an embayment surrounded by heavily industrialized cities, Korea. *Science of the Total Environment*, *407*(9), 3181–3188. https://doi.org/10.1016/j.scitotenv.2008.04.013

Li, H. M., Tang, H. J., Shi, X. Y., Zhang, C. S., & Wang, X. L. (2014). Increased nutrient loads from the Changjiang (Yangtze) River have led to increased Harmful Algal Blooms. *Harmful Algae*, *39*(39), 92–101.

Lian, E., Yang, S., Wu, H., Yang, C., Li, C., & Liu, J. T. (2016). Kuroshio subsurface water feeds the wintertime Taiwan Warm Current on the inner East China Sea shelf. *Journal of Geophysical Research: C Oceans*, *121*, 4790–4803. https://doi.org/10.1002/2016JC011869

Liu, J. P., Li, A. C., Xu, K. H., Velozzi, D. M., Yang, Z. S., Milliman, J. D., & DeMaster, D. J. (2006). Sedimentary features of the Yangtze River-derived along-shelf clinoform deposit in the East China Sea. *Continental Shelf Research*, *26*(17–18), 2141–2156. https://doi.org/10.1016/j.csr.2006.07.013

Liu, J. P., Xu, K. H., Li, A. C., Milliman, J. D., Velozzi, D. M., Xiao, S. B., & Yang, Z. S. (2007). Flux and fate of Yangtze River sediment delivered to the East China Sea. *Geomorphology*, *85*(3–4), 208–224. https://doi.org/10.1016/j.geomorph.2006.03.023

Liu, Q., Charette, M. A., Henderson, P. B., McCorkle, D. C., Martin, W., & Dai, M. (2014). Effect of submarine groundwater discharge on the coastal ocean inorganic carbon cycle. *Limnology and Oceanography: Methods*, *59*(5), 1529–1554. https://doi.org/10.4319/lo.2014.59.5.1529

Liu, Q., Dai, M., Chen, W., Huh, C. A., Wang, G., Li, Q., & Charette, M. A. (2012). How significant is submarine groundwater discharge and its associated dissolved inorganic carbon in a river-dominated shelf system? *Biogeosciences*, *9*(5), 1777–1795. https://doi.org/10.5194/bg-9-1777-2012

Liu, Z., & Gan, J. (2012). Variability of the Kuroshio in the East China Sea derived from satellite altimetry data. *Deep Sea Research Part I: Oceanographic Research Papers*, *59*, 25–36. https://doi.org/10.1016/j.dsr.2011.10.008

Lucas, H. F. (1957). Improved low-level alpha-scintillation counter for radon. *Review of Scientific Instruments*, *28*(9), 680–683. https://doi.org/10.1063/1.1715975

Luo, Y., Lao, H., & Wang, L. (1985). A preliminary study on the surface sediment types and their grain size characteristics of the northeastern part of the South China Sea [in Chinese]. *Journal of Tropical Oceanography*, *4*(1), 33–41.

Mao, Z., & Shen, H. (2001). Comparative study of turbidity maximum in the Changjiang and Oujiang estuaries. *Marine Science Bulletin*, *20*(3), 8–14.

Milliman, J. D., & Meade, R. H. (1983). World-wide delivery of river sediment to the oceans. *Journal of Geology*, *91*(1), 1–21. https://doi.org/10.1086/628741

Ministry of Water Resources of PRC (Ed.) (2010). *China river sediment bulletin 2009* (pp. 68). Beijing, China: China Water Power Press. Retrieved from http://www.mwr.gov.cn/sj/tjgb/zghlnsgb/201612/t20161222_776064.html

Moore, W. S. (1976). Sampling ^{228}Ra in the deep ocean. *Deep Sea Research and Oceanographic Abstracts*, *23*(7), 647–651. https://doi.org/10.1016/0011-7471(76)90007-3

Moore, W. S. (1984). Radium isotope measurements using germanium detectors. *Nuclear Instruments and Methods in Physics Research*, *223*(2–3), 407–411. https://doi.org/10.1016/0167-5087(84)90683-5

Moore, W. S. (1998). Application of ^{226}Ra, ^{228}Ra, ^{223}Ra, and ^{224}Ra in coastal waters to assessing coastal mixing rates and groundwater discharge to oceans. *Journal of Earth System Sciences*, *107*(4), 1–7. https://doi.org/10.1007/BF02841600

Moore, W. S. (1999). The subterranean estuary: A reaction zone of ground water and sea water. *Marine Chemistry*, *65*(1–2), 111–125. https://doi.org/10.1016/S0304-4203(99)00014-6

Moore, W. S. (2000a). Ages of continental shelf waters determined from ^{223}Ra and ^{224}Ra. *Journal of Geophysical Research*, *105*(C9), 22117–22122. https://doi.org/10.1029/1999JC000289

Moore, W. S. (2000b). Determining coastal mixing rates using radium isotopes. *Continental Shelf Research*, *20*(15), 1993–2007. https://doi.org/10.1016/S0278-4343(00)00054-6

Moore, W. S. (2003). Sources and fluxes of submarine groundwater discharge delineated by radium isotopes. *Biogeochemistry*, *66*(1–2), 75–93. https://doi.org/10.1023/B:BIOG.0000006065.77764.a0

Moore, W. S. (2006). Radium isotopes as tracers of submarine groundwater discharge in Sicily. *Continental Shelf Research*, *26*(7), 852–861. https://doi.org/10.1016/j.csr.2005.12.004

Moore, W. S. (2007). Seasonal distribution and flux of radium isotopes on the southeastern U.S. continental shelf. *Journal of Geophysical Research*, *112*, C10013. https://doi.org/10.1029/2007JC004199

Moore, W. S. (2008). Fifteen years experience in measuring ^{224}Ra and ^{223}Ra by delayed-coincidence counting. *Marine Chemistry*, *109*(3–4), 188–197. https://doi.org/10.1016/j.marchem.2007.06.015

Moore, W. S. (2010a). The effect of submarine groundwater discharge on the ocean. *Annual Review of Marine Sciences*, *2*, 59–88. https://doi.org/10.1146/annurev-marine-120308-081019

Moore, W. S. (2010b). A reevaluation of submarine groundwater discharge along the southeastern coast of North America. *Global Biogeochemical Cycles*, *24*, GB4005. https://doi.org/10.1029/2009GB003747

Moore, W. S., & Arnold, R. (1996). Measurement of ^{223}Ra and ^{224}Ra in coastal waters using a delayed coincidence counter. *Journal of Geophysical Research*, *101*(C1), 1321–1329. https://doi.org/10.1029/95JC03139

Moore, W. S., Blanton, J. O., & Joye, S. B. (2006). Estimates of flushing times, submarine groundwater discharge, and nutrient fluxes to Okatee Estuary, South Carolina. *Journal of Geophysical Research*, *111*, C09006. https://doi.org/10.1029/2005JC003041

Moore, W. S., & Cai, P. (2013). Calibration of RaDeCC systems for ^{223}Ra measurements. *Marine Chemistry*, *156*, 130–137. https://doi.org/10.1016/j.marchem.2013.03.002

Moore, W. S., & de Oliveira, J. (2008). Determination of residence time and mixing processes of the Ubatuba, Brazil, inner shelf waters using natural Ra isotopes. *Estuarine, Coastal Shelf Science*, *76*(3), 512–521. https://doi.org/10.1016/j.ecss.2007.07.042

Moore, W. S., Key, R. M., & Sarmiento, J. L. (1985). Techniques for precise mapping of ^{226}Ra and ^{228}Ra in the ocean. *Journal of Geophysical Research*, *90*(C4), 6983–6994. https://doi.org/10.1029/JC090iC04p06983

Moore, W. S., & Krest, J. (2004). Distribution of ^{223}Ra and ^{224}Ra in the plumes of the Mississippi and Atchafalaya Rivers and the Gulf of Mexico. *Marine Chemistry*, *86*(3–4), 105–119. https://doi.org/10.1016/j.marchem.2003.10.001

Moore, W. S., Sarmiento, J. L., & Key, R. M. (2008). Submarine groundwater discharge revealed by ^{228}Ra distribution in the upper Atlantic Ocean. *Nature Geoscience*, *1*(5), 309–311. https://doi.org/10.1038/ngeo183

Niino, H., & Emery, K. O. (1961). Sediments of shallow portions of East China Sea and South China Sea. *Geological Society of American Bulletin*, *72*(5), 731–762. https://doi.org/10.1130/0016-7606(1961)72[731:SOSPOE]20.CO;2

Pan, A., Wan, X., Guo, X., & Jing, C. (2012). Responses of the Zhe-Min coastal current adjacent to Pingtan Island to the wintertime monsoon relaxation in 2006 and its mechanism. *Science China: Earth Sciences*, *56*(3), 386–396. https://doi.org/10.1007/s11430-012-4429-9

Rapaglia, J., Koukoulas, S., Zaggia, L., Lichter, M., Manfé, G., & Vafeidis, A. T. (2012). Quantification of submarine groundwater discharge and optimal radium sampling distribution in the Lesina Lagoon, Italy. *Journal of Marine Systems*, *91*(1), 11–19. https://doi.org/10.1016/j.jmarsys.2011.09.003

Rodellas, V., Garcia-Orellana, J., Masqué, P., Feldman, M., & Weinstein, Y. (2015). Submarine groundwater discharge as a major source of nutrients to the Mediterranean Sea. *Proceedings of the National Academy of Sciences of the United States of America*, *112*(13), 3926–3930. https://doi.org/10.1073/pnas.1419049112

Sanders, C. J., Santos, I. R., Barcellos, R., & Silva Filho, E. V. (2012). Elevated concentrations of dissolved Ba, Fe and Mn in a mangrove subterranean estuary: Consequence of sea level rise? *Continental Shelf Research*, *43*, 86–94. https://doi.org/10.1016/j.csr.2012.04.015

Smith, C. G., & Swarzenski, P. W. (2012). An investigation of submarine groundwater-borne nutrient fluxes to the west Florida shelf and recurrent harmful algal blooms. *Limnology and Oceanography*, *57*(2), 471–485. https://doi.org/10.4319/lo.2012.57.2.0471

Smoak, J. M., Sanders, C. J., Patchineelam, S. R., & Moore, W. S. (2012). Radium mass balance and submarine groundwater discharge in Sepetiba Bay, Rio de Janeiro State, Brazil. *Journal of South American Earth Sciences*, *39*, 44–51. https://doi.org/10.1016/j.jsames.2012.07.004

Street, J. H., Knee, K. L., Grossman, E. E., & Paytan, A. (2008). Submarine groundwater discharge and nutrient addition to the coastal zone and coral reefs of leeward Hawai'i. *Marine Chemistry*, *109*(3–4), 355–376. https://doi.org/10.1016/j.marchem.2007.08.009

Su, N., Du, J., Duan, Z., Deng, B., & Zhang, J. (2015). Radium isotopes and their environmental implications in the Changjiang River system. *Estuarine, Coastal and Shelf Science*, *156*, 155–164. https://doi.org/10.1093/annonc/mdu326.14

Valiela, I., Costa, J., Foreman, K., Teal, J., Howes, B., & Aubrey, D. (1990). Transport of groundwater-borne nutrients from watersheds and their effects on coastal waters. *Biogeochemistry*, *10*(3), 177–197. https://doi.org/10.1007/BF00003143

Wang, G., Jing, W., Wang, S., Xu, Y., Wang, Z., Zhang, Z., Li, Q., & Dai, M. (2014). Coastal acidification induced by tidal-driven submarine groundwater discharge in a coastal coral reef system. *Environmental Science & Technology*, *48*(22), 13069–13075. https://doi.org/10.1021/es5026867

Wang, G., Wang, Z., Zhai, W., Moore, W. S., Li, Q., Yan, X., Qi, D., & Jiang, Y. (2015). Net subterranean estuarine export fluxes of dissolved inorganic C, N, P, Si, and total alkalinity into the Jiulong River estuary, China. *Geochimica et Cosmochimica Acta*, *149*, 103–114. https://doi.org/10.1016/j.gca.2014.11.001

Wang, L., Yu, R., Hu, G., & Tu, X. (2010). Speciation and assessment of heavy metals in surface sediments of Jinjiang river tidal reach, southeast of China. *Environmental Monitoring and Assessment*, *165*(1–4), 491.

Wang, S. L. (2014). *Submarine groundwater discharge and associated fluxes of nutrients and carbon into the Pearl River estuary* (Master thesis). Xiamen University, Xiamen, Fujian Province, China.

Windom, H. L., Moore, W. S., Niencheski, L. F. H., & Jahnke, R. A. (2006). Submarine groundwater discharge: A large, previously unrecognized source of dissolved iron to the South Atlantic Ocean. *Marine Chemistry*, *102*(C9), 252–266. https://doi.org/10.1016/j.marchem.2006.06.016

Zhai, W., Dai, M., & Guo, X. (2007). Carbonate system and CO_2 degassing fluxes in the inner estuary of Changjiang (Yangtze) River, China. *Marine Chemistry*, *107*(3), 342–356. https://doi.org/10.1016/j.marchem.2007.02.011

Zhang, C. Y., Shang, S. L., & Chen, D. W. (2005). Short-term variability of the distribution of Zhe-Min coastal water and wind forcing during winter monsoon in the Taiwan Strait (in Chinese). *Journal of Remote. Sensing*, *9*(4), 452–458.

Zhang, F., Zhang, W., & Yang, Q. (2003). Characteristics of grain size distributions of surface sediments in the eastern South China Sea (in Chinese). *Acta Sedimentologica Sinica*, *21*, 452–460.